06

Memristor nanostructures based on the bigraphene/diamane phase transition

© G.N. Panin,[1] E.V. Emelin,[1] O.O. Kapitanova,[2,3] V.I. Korepanov,[1] L.A. Varlamova,[4] D.O. Klimchuk,[4] S.V. Erokhin,[4] K.V. Larionov,[4] P.B. Sorokin[1,4]

[1] Institute of Microelectronics Technology and High-Purity Materials
142432 Chernogolovka, Moscow region, Russia
[2]Department of Chemistry, Moscow State University,
119991 Moscow, Russia
[3] Center for Photonics and 2D Materials, Moscow Institute of Physics and Technology,
141701 Dolgoprudny, Moscow region, Russia
[4] Laboratory of Digital Materials Science, National University of Science and Technology MISIS,
119049 Moscow, Russia
e-mail: panin@iptm.ru

Received October 24, 2024
Revised October 24, 2024
Accepted October 24, 2024

Carbon nanostructures based on a local structural phase transition bigraphene/diamane obtained by transferring two graphene layers onto a $La_3Ga_5SiO_{14}$ substrate and irradiating them with an electron beam through a polymethyl methacrylate layer are studied. Irradiation of the structure led to local functionalization of bigraphene with oxygen and hydrogen with the formation of sp^3- bonds and a bigraphene–diamane phase transition, which was previously predicted theoretically. Changes in the intensity and position of peaks in the Raman spectra of irradiated bigraphene and an increase in its resistance indicate a local phase transition. Theoretical calculations of the modified bigraphene structure on $La_3Ga_5SiO_{14}$ and experimental measurements of the proportion of sp^3-hybridized carbon atoms indicate the formation of diamane nanoclusters and the possibility of local formation of nanostructures whose memristive states can be controlled at low currents and bias voltages.

Keywords: graphene, diamond monolayer, memristor, electron beam nanotechnology, low-dimensional crystals.

DOI: 10.61011/TP.2025.02.60835.359-24

Introduction

The need to process large volumes of data in real time by artificial intelligence systems of self-driving vehicles encourages researchers to create more energy-efficient and faster microelectronic components. DOJO processor developed in 2021 for Tesla Autopilot neural artificial vision networks on the basis of 7 nm CMOS (complementary metal-oxide-semiconductor) technology has a set of $D1$ boards with 25 integrated circuits each that consume 15 kW (288 A, 52 V) (Figure 1) [1]. To perform $\sim 10^{18}$ operations per 1 s (1.1 EFLOP), the processor needs 3000 $D1$ boards with the total power consumption of 45 MW. The annual consumption peak of electricity produced by heat, hydroelectric, nuclear, solar and wind power plants in the Unified Energy System of Russia in 2021 was ~ 161000 MW [2] which may supply power to ~ 3500 autopilots. This is by orders of magnitude lower that the number of traditional drivers on the roads in Saint Petersburg (2.5 mln) or Moscow (5 mln). An ordinary driver brain consumes 10−20 W. The data indicates low energy efficiency of artificial real-time data processing systems and the need for their development.

With the emergence of new low-dimensional crystals and memristor nanostructures based on them that have unique structural, electronic and optical properties, electronic and optoelectronic devices with better energy efficiency and data processing rate may be created. Two-dimensional graphene-like crystals [3] and Van der Waals heterostructures [4] have high mobility of charge carriers and cover a wide ultraviolet, visible and infrared absorption spectral range [5]. An important feature of two-dimensional crystals is the absence of dangling bonds on their surface, which makes it possible to build them in CMOS to form defect-free interfaces. Using the CMOS technology, high performance photosensors with high resolution and sensitivity in a wide range from 300 nm to 2 μm were demonstrated [6].

Two-dimensional crystals also demonstrate ultra-fast photoinduced structural phase transitions [7–11]. For example, reversible photoinduced phase transition in MoS_2 from semiconductor phase 2H to metallic phase 1T (Figure 2) may occur during ultrashort times in a femtosecond range [12].

This approach was used to demonstrate dynamic switching of the MoS_2 QDNS photomemristor structure (two-dimensional nanocrystals with quantum dots) [13,14]. Photomemristive states associated with 2H- and 1T-phases are well controlled by 532 nm light and the bias voltage of 1.7 V and 2.7 V [13]. Resistive switching was also observed in electric field in a graphene oxide (GO) structure [15–18].

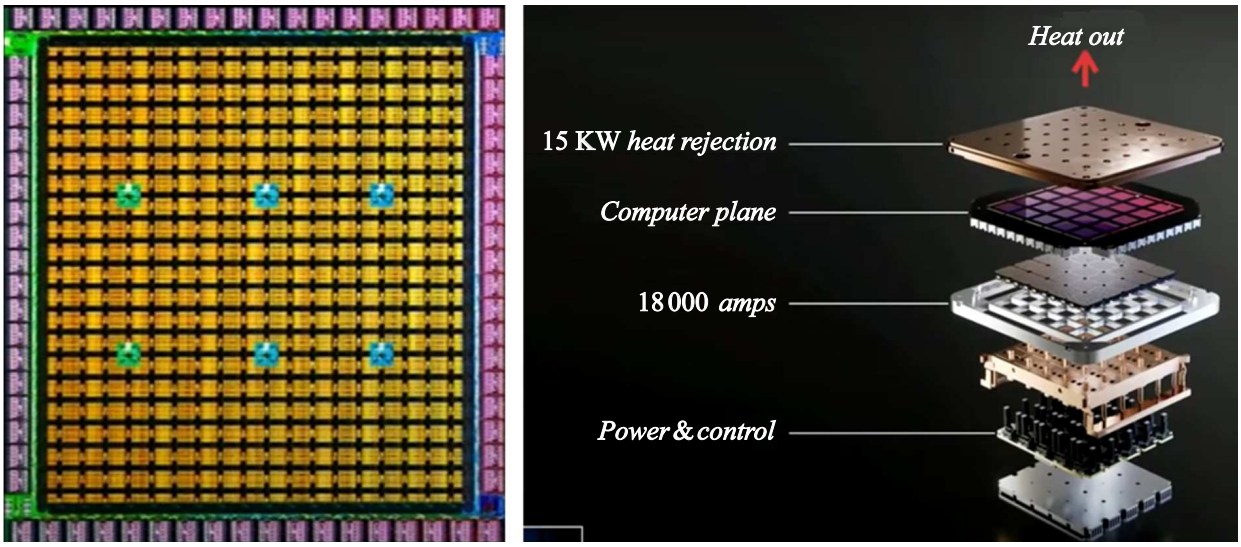

Figure 1. Boards with 25 integrated circuits with DOJO processors intended for neural networks for pattern recognition in the Tesla Autopilot artificial intelligence system (left). Power of each board (right) is 15 kW.

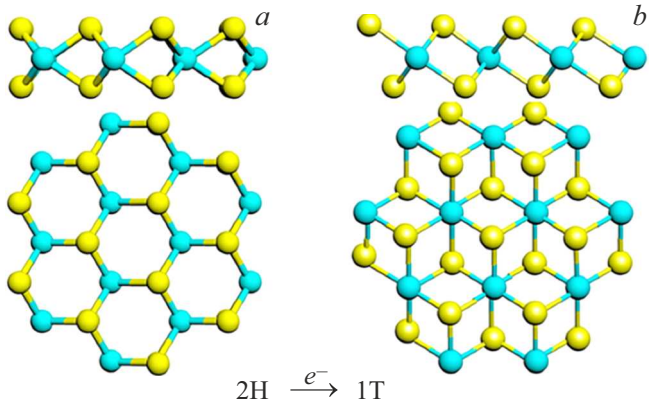

Figure 2. Phase transition in two-dimensional MoS_2 from semiconductor phase 2H (a) to metallic phase 1T (b) [7].

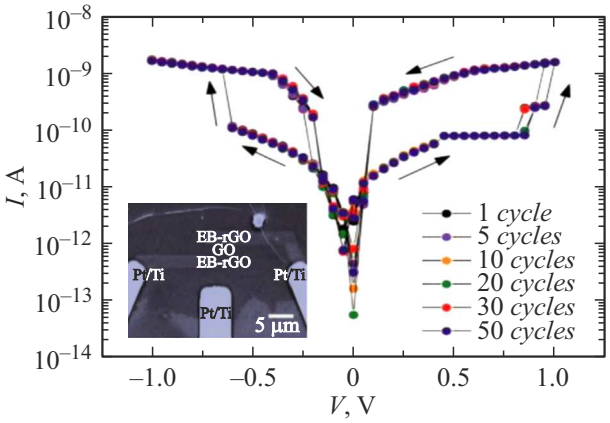

Figure 3. I-V characteristics of the PtTi/rGO/GO/rGO/PtTi memristor structure formed by an electron beam (inset) and cyclic switching of resistive states associated with sp^3- and sp^2-hybridization of carbon atoms, by the bias voltage of 0.8–0.9 V.

At low bias voltages (0.4 V), resistance in the Al/GO/Al memristor nanostructures varied by three orders of magnitude. Detailed analysis of such structures showed that resistive switching was associated with conductive channels in graphene oxide that are formed during tuning of the sp^3/sp^2-hybridization of carbon atoms [19]. Memristive states in the PtTi/GO/PtTi nanostructures made by electron beam irradiation [14,19] are well controlled by the bias voltage of < 1 V (Figure 3) and allow signal processing in memory [20–27].

Such approach may be used for energy-efficient processing of large amounts of electrical [28–30] and optical [31] data.

1. Bigraphene/diamond-like C_2H-diamane phase transition

Phase transition of hydrogen-bonded bigraphene to diamond-like C_2H-diamane was predicted by L.A. Chernozatonsky et al [32]. Atomic structures of single-layer graphane (a) and diamane (b) are shown in Figure 4.

Hydrogen atom adsorption by graphene and bigraphene leads to formation of materials with new electronic properties, in particular, to single-layer diamond (diamane).

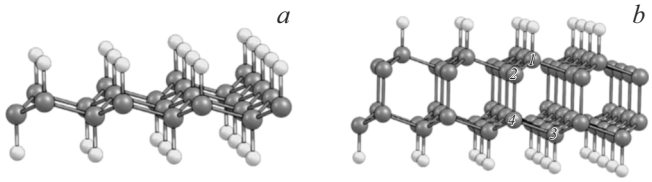

Figure 4. Atomic structures of single-layer graphane (a) and diamane (b).

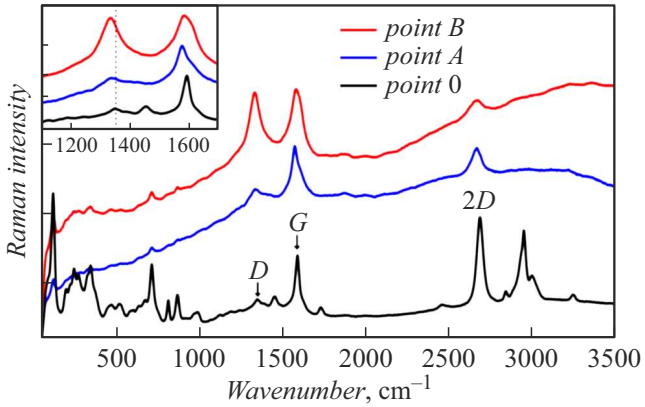

Figure 5. Raman scattering spectra of locally electron-beam irradiated bigraphene at different irradiation doses ($D_B > D_A > D_0$).

Chemically induced phase transition of bilayer graphene to single-layer diamond was confirmed experimentally by CVD-bigraphene fluorination [33]. Methods with high spatial resolution demonstrated formation of interlayer carbon-carbon bonds and fluorinated diamond monolayer (F-diamane).

2. Local bigraphene/diamane phase transition induced by electron beam

Local phase transition in a structure based on bigraphene transferred to a $La_3Ga_5SiO_{14}$ substrate was achieved by electron-beam irradiation through polymethyl methacrylate (PMMA) [34]. Phase transition of bilayer graphene to diamane was observed when hydrogen and oxygen atoms were released from PMMA and langasite, respectively, and bonded in local irradiated regions with bigraphene. Raman scattering (RS) spectra of bigraphene locally electron-beam irradiated with different irradiation doses show that, as the dose increases, the ratio of typical peaks D to G increases (Figure 5).

Variation of peak intensity and position in RS spectra and increase in bigraphene resistance after irradiation indicate local phase transition of bigraphene to diamane with the sp^3-hybridization of carbon atoms. Raman mapping of the bigraphene/diamane/bigraphene structure shows that local phase transition is formed and the fraction of carbon atoms in the sp^3-hybridization in the irradiated region increases to $3 \cdot 10^{11}$ cm^{-2} (Figure 6).

Modeling of the modified bigraphene structure on $La_3Ga_5SiO_{14}$ and experimental evaluation of the sp^3-hybridized carbon atom fraction indicate that diamane

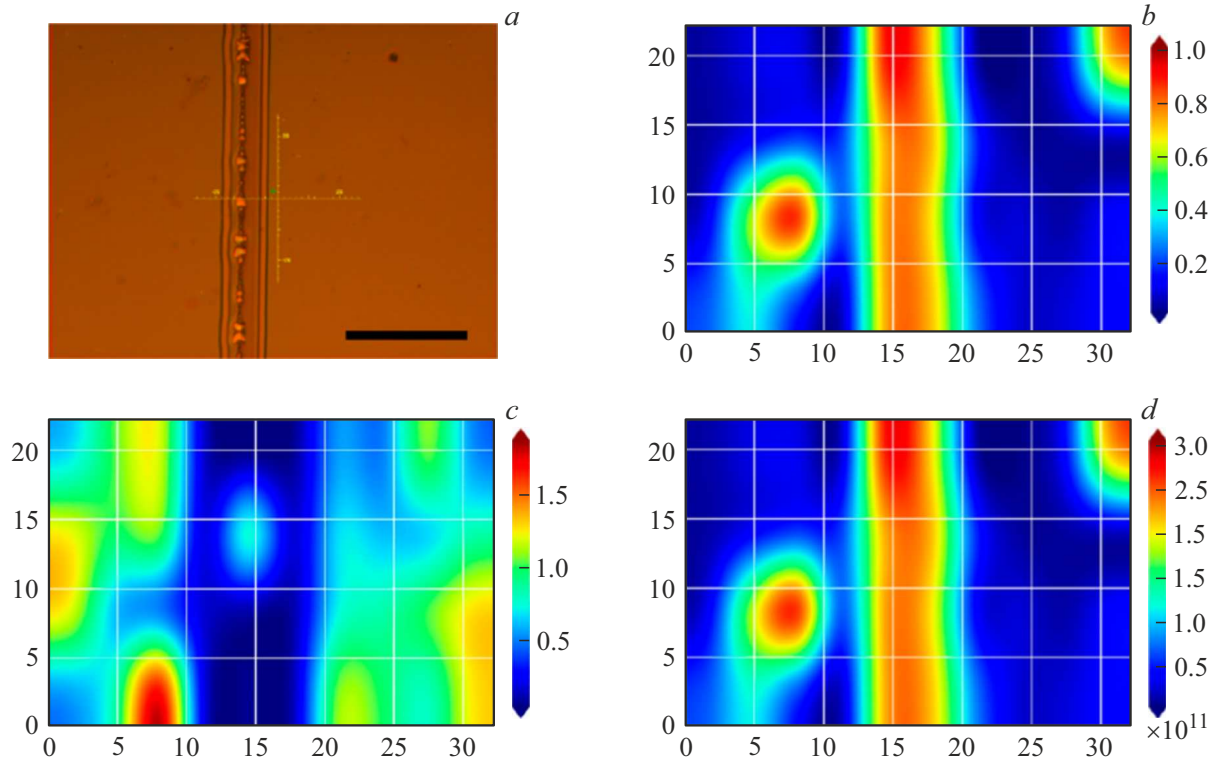

Figure 6. Raman mapping of the bigraphene/diamane/bigraphene nanostructure obtained by irradiation of bigraphene on $La_3Ga_5SiO_{14}$ through PMMA. Optical image of the bilayer graphene surface irradiated with electron beam (vertical band) at the accelerating voltage of 25 kV and dose of 1 μC/cm^2 (a). Scale bar — 1 μm. Intensity ratio map of Raman bands D and G (b), $2D$ and G (c) of the bilayer graphene after local electron irradiation in the form of a vertical band. Distribution of defect density sp^3 (cm^{-2}) evaluated by the D-peak (d).

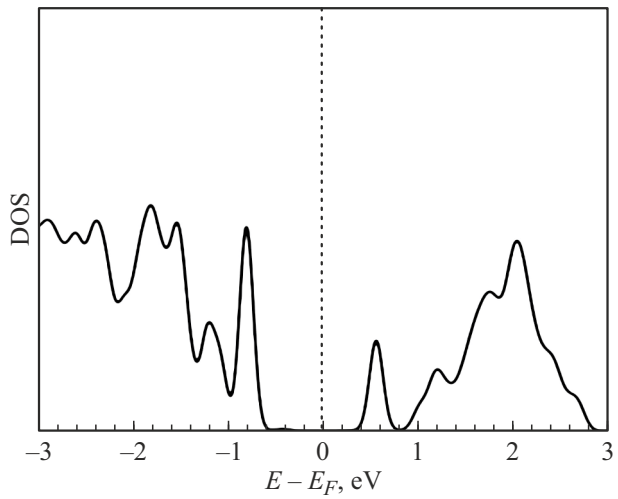

Figure 7. Density of electron states of diamane (carbon and hydrogen atoms) in the diamane/langasite nanostructure. Fermi level is shifted to zero.

clusters are formed in the irradiated bigraphene regions and the band gap is opened in bigraphene at the level of 0.7 eV (Figure 7) [34].

3. Memristor nanostructures based on the bigraphene/diamane phase transition

Memristor nanostructures were made using local bigraphene/diamane phase transition. Electron beam irradiation dose needed to destroy PMMA and release hydrogen from it and oxygen from the $La_3Ga_5SiO_{14}$ substrate was measured experimentally and used for direct electron-beam formation of memristor nanostructures. The formation scheme and optical image of the AlCr/bigraphene/diamane /bigraphene/AlCr nanostructure obtained by electron beam scanning through PMMA at optimal irradiation parameters ($U = 25$ kV, $D = 1$ mC/cm^2) along a line with a width of 200 nm, as well as the current-voltage (I-V) characteristics of the structure before and after are shown in Figure 8.

Bigraphene on the $La_3Ga_5SiO_{14}$ substrate was produced by transferring graphene grown on copper foil by the CVD method described earlier in [34,35]. Electron-beam induced phase transition of bigraphene to diamane leads to formation of a barrier for charge carriers and nonlinear I-V characteristics (Figure 8, bottom right inset). I-V characteristics and resistance variation in the Al(Cr)/bigraphene/Al(Cr) structure non-irradiated and locally electron-beam irradiated along the line show that irradiation of the structure lead to a nonlinear dependence of current on bias voltage and to increase in resistance by two orders of magnitude. AlCr/bigraphene/diamane/bigraphene/AlCr memristor nanostructure formed by the electron beam in bigraphene shows nonvolatile memristive states of bigraphene (420 Ω)

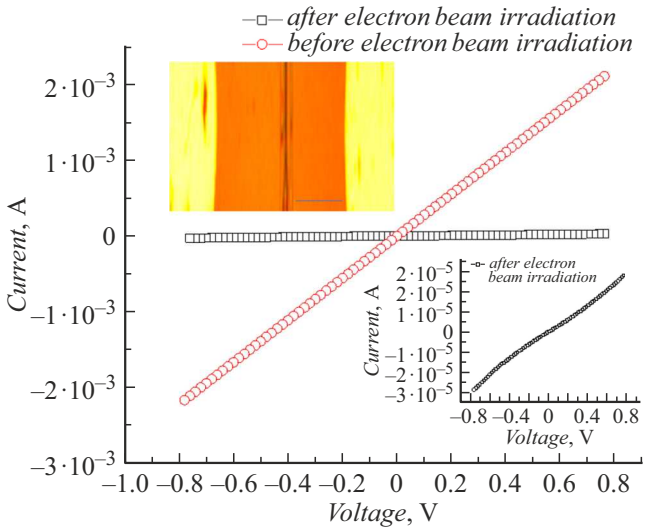

Figure 8. The current-voltage characteristics of the AlCr/bigraphene/AlCr/ nanostructure on the $La_3Ga_5SiO_{14}$ substrate before electron beam irradiation (red open circles) and after irradiation of the ∼ 200 nm region (dark vertical band in the top left inset) open squares). Inset — optical image of the nanostructure: bigraphene — brown, Al/Cr electrodes — yellow. Bigraphene — diamane region after local electron-beam irradiation — vertical dark band. Scale bar — 1000 nm. Insert at the bottom right — I-V characteristics of the obtained nanostructure in the region of low currents after irradiation with an electron beam.

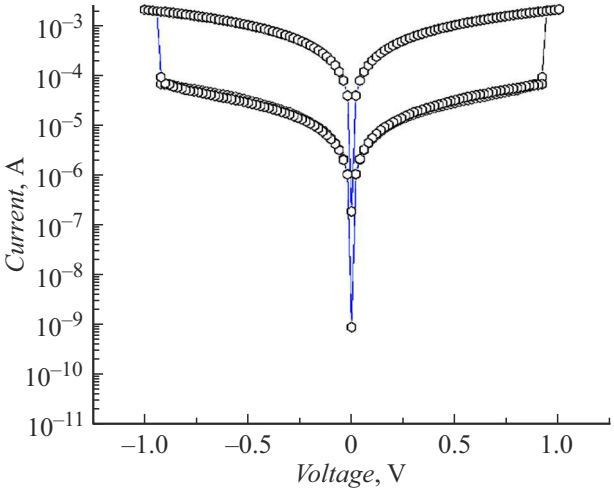

Figure 9. Switching of memristive states of the bigraphene/diamane/bigraphene nanostructure with AlCr electrode on the $La_3Ga_5SiO_{14}$ substrate formed by electron-beam irradiation of bigraphene at the bias voltages of ±0.9 V.

and diamane (20 kΩ) (Figure 9), which can be reversibly switched in an electric field at bias voltages of ±0.9 V.

Modeling and evaluation of the stability of the bigraphene/diamane structure in an electric field show that diamane with a minimum width of 1 nm is thermodynamically stable (Figure 10).

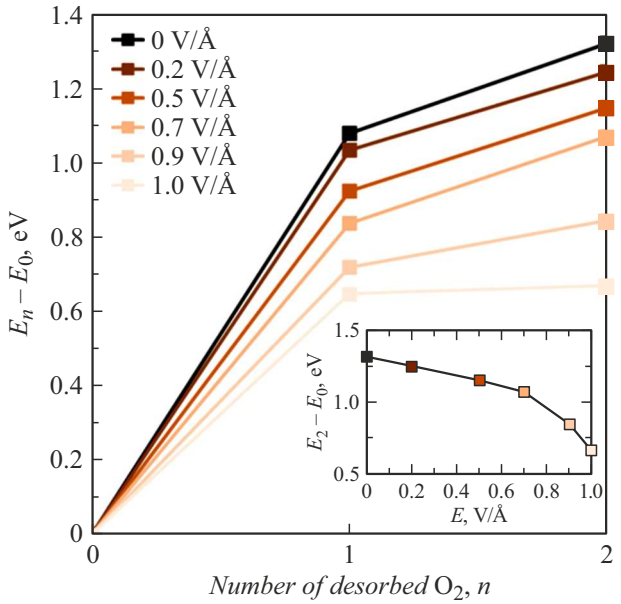

Figure 10. Dependence of the diamond cleavage barrier calculated as the difference between the initial stage and the stage with detached O_2 for the desorption of one and two oxygen molecules from the diamond surface. The graph shows cleavage barrier variation at different applied electric field values. The inset shows in more detail the dependence of the cleavage barrier during the desorption of two oxygen molecules on the applied electric field.

When the band width is < 1 nm, the structure becomes instable and is separated into bilayer graphene. As the band width increases, the energy barrier for diamond cluster cleavage grows from 0.66 eV/O_2 to 2.38 eV/O_2 [36]. The obtained data indicates that phase transition can be controlled in nanoscale memristor structures in the electric field that decreases as the structure sizes decrease.

Conclusions

Local phase transition from bigraphene to diamane predicted theoretically was studied experimentally. Electron-beam irradiation of the PMMA/bigraphene/langasite structure in optimum conditions leads to formation of hydrogen and oxygen atoms and their binding with bigraphene in the irradiated regions to form diamane. Low-dimensional structures based on bigraphene/diamane represent a new class of atomic functional devices obtained by direct electron beam exposure compatible with CMOS technology and promising for the creation of new energy-efficient multi-level resistive memory.

Funding

This study was supported financially by the Russian Science Foundation, project No. 23-49-00159. Work on experimental facilities of the Institute of Microelectronics Technology and High-Purity Materials of the Russian Academy of Sciences was carried out and supported within the framework of a state assignment № 075-00295-25-00.

Conflict of interest

The authors declare no conflict of interest.

References

[1] T.P. Morgan. *The Next Platform* (August 23, 2022), https://www.nextplatform.com/2022/08/23/inside-teslas-innovative-and-homegrown-dojo-ai-supercomputer/
[2] *SO UPS data on electricity consumption in the Unified Power System of Russia*, Electronic source. Available at: https://www.so-ups.ru/news/press-release/press- release-view/news/17511/
[3] K.S. Novoselov, A.K. Geim, S.V. Morozov, D. Jiang, Y. Zhang, S.V. Dubonos, I.V. Grigorieva, A.A. Firsov. Science, **306**, 666 (2004). DOI: 10.1126/science.1102896
[4] A.K. Geim, I.V. Grigorieva. Nature, **499**, 419 (2013). DOI: 10.1038/nature12385
[5] X. Cai, Y. Luo, B. Liu, H.M. Cheng. Chem. Soc. Rev., **47**, 6224 (2018). DOI: 10.1039/C8CS00254A
[6] S. Goossens, G. Navickaite, C. Monasterio, S. Gupta, J.J. Piqueras, R. Pérez, G. Burwell, I. Nikitskiy, T. Lasanta, T. Galán, E. Puma, A. Centeno, A. Pesquera, A. Zurutuza, G. Konstantatos, F. Koppens. Nature Photon., **11**, 366 (2017). DOI: 10.1038/nphoton.2017.75
[7] Y. Guo, D. Sun, B. Ouyang, A. Raja, J. Song, T.F. Heinz, L.E. Brus. Nano Lett., **15**, 5081 (2015). DOI: 10.1021/acs.nanolett.5b01196
[8] K. Nasu. *Photoinduced Phase Transitions* (World Scientific, Singapore 2004), DOI: 10.1142/5476
[9] B. Peng, H. Zhang, W. Chen, B. Hou, Z-J. Qiu, H. Shao, H. Zhu, B. Monserrat, D. Fu, H. Weng, C.M. Soukoulis. 2D Mater. Appl., **4**, 14 (2020). DOI: 10.1038/s41699-020-0147-x
[10] Y. Cheng, A. Nie, Q. Zhang, L-Y. Gan, R. Shahbazian-Yassar, U. Schwingenschlogl. ACS Nano, **8** (11), 11447 (2014). DOI: 10.1021/nn505668c
[11] P. Byrley, M. Liu, R. Yan. Front. Chem., **7**, 442 (2019). DOI: 10.3389/fchem.2019.00442
[12] X. Li, L. Tao, Z. Chen, H. Fang, X. S. Li, X. Wang, J.B. Xu, H. Zhu. Appl. Phys. Rev., **4**, 021306 (2017). DOI: 10.1063/1.4983646
[13] X. Fu, L. Zhang, H.D. Cho, T.W. Kang, D. Fu, D. Lee, S.W. Lee, L. Li, T. Qi, A.S. Chan, Z.A. Yunusov, G.N. Panin. Small, **15** (45), 1903809 (2019). DOI: 10.1002/smll.201903809
[14] G.N. Panin. Chaos, Solitons and Fractals, **142**, 110523 (2021). DOI: 10.1016/j.chaos.2020.110523
[15] C.L. He, F. Zhuge, X.F. Zhou, M. Li, G.C. Zhou, Y.W. Liu, J.Z. Wang, B. Chen, W.J. Su, Z.P. Liu, Y.H. Wu, P. Cui, R.-W. Li. Appl. Phys. Lett., **95**, 232101 (2009). DOI: 10.1063/1.3271177
[16] H.Y. Jeong, J.Y. Kim, J.W. Kim, J.O. Hwang, J.-E. Kim, J.Y. Lee, T.H.Yoon, B.J. Cho, S.O. Kim, R.S. Ruoff, S.-Y. Choi. Nano Lett., **10**, 4381 (2010). DOI: 10.1021/nl101902k
[17] G.N. Panin, O.O. Kapitanova, S.W. Lee, A.N. Baranov, T.W. Kang. Jpn., J. Appl. Phys., **50**, 070110 (2011). DOI: 10.3938/jkps.64.1399

[18] O.O. Kapitanova, G.N. Panin, O.V. Kononenko, A.N. Baranov, T.W. Kang. J. Kor. Phys. Soc., **64**, 1399 (2014). DOI: 10.3938/jkps.64.1399
[19] O.O. Kapitanova, E.V. Emelin, S.G. Dorofeev, P.V. Evdokimov, G.N. Panin, Y. Lee, S. Lee. J. Mat. Sci. Tech., **38**, 237 (2020). DOI: 10.1016/j.jmst.2019.07.042
[20] S. Ghose. IBM J. Research and Development, **63** (6), 3:1 (2019). DOI: 10.1147/JRD.2019.2934048
[21] Z. Hao, G. Chen, B. C. Ooi, K.-L. Tan, M. Zhang. IEEE Transactions on Knowledge and Data Engineering, **27** (7) 1920 (2015). DOI: 10.1109/TKDE.2015.2427795
[22] H. Plattner, A. Zeier. *In-Memory Data Management: Technology and Applications* (Springer Science & Business Media, 2012)
[23] S.E. Fatemieh, M.R. Reshadinezhad, N. Taherinejad. *IEEE International Symposium on Circuits and Systems (ISCAS)* (2022), p. 3115. DOI: 10.1109/ISCAS48785.2022.9937475
[24] S.-G. Ren, A. Dong, L. Yang, Y.-B. Xue, J.-C. Li, Y.-J. Yu, H.-J. Zhou, W.-B. Zuo, Y. Li, W.-M. Cheng, X.-S. Miao. Adv. Mater., **36**, 2307218 (2024). DOI: 10.1002/adma.202307218
[25] C. Li, C. Li, D. Belkin, Y. Li, P. Yan, M. Hu, N. Ge, H. Jiang, E. Montgomery, P. Lin, Z. Wang, J.P. Strachan, M. Barnell, Q. Wu, R.S. Williams, J.J. Yang, Q. Xia. *IEEE International Memory Workshop (IMW)* (Kyoto, Japan, 2018), p. 1–4. DOI: 10.1109/IMW.2018.8388838
[26] A. Mehonic, A. Sebastian, B. Rajendran, O. Simeone, E. Vasilaki, A.J. Kenyon. Adv. Intell. Syst., **2**, 2000085 (2020). DOI: 10.1002/aisy.202000085
[27] L.O. Chua. Nat Electron, **1**, 322 (2018). DOI: 10.1038/s41928-018-0074-4
[28] L. Chua. IEEE Transactions on Circuit Theory, **18** (5), 507 (1971). DOI: 10.1109/TCT.1971.1083337
[29] B. Kim, H. Li, Y. Chen. *GLSVLSI '24: Proceedings of the Great Lakes Symposium on VLSI 2024* (2024), p. 614. DOI: 10.1145/3649476.3660367
[30] G.N. Panin. Electronics, **11**, 619 (2022). DOI: 10.3390/electronics11040619
[31] X. Fu, T. Li, B. Cai, J. Miao, G.N. Panin, X. Ma, J. Wang, X. Jiang, Q. Li, Y. Dong, C. Hao, J. Sun, H. Xu, Q. Zhao, M. Xia, B. Song, F. Chen, X. Chen, W. Lu, W. Hu. Light Sci. Appl., **12**, 39 (2023). DOI: 10.1038/s41377-023-01079-5
[32] L.A. Chernozatonskii, P.B. Sorokin, A.G. Kvashnin, D.G. Kvashnin. JETP Lett., **90**, 134 (2009). DOI: 10.1134/S0021364009140112
[33] P.V. Bakharev, M. Huang, M. Saxena, S.W. Lee, S.H. Joo, S.O. Park, J. Dong, D.C. Camacho-Mojica, S. Jin, Y. Kwon, M. Biswal, F. Ding, S.K. Kwak, Z. Lee, R.S. Ruoff. Nat. Nanotechnol., **15**, 59 (2020). DOI: 10.1038/s41565-019-0582-z
[34] E.V. Emelin, H.D. Cho, V.I. Korepanov, L.A. Varlamova, S.V. Erohin, D.Y. Kim, P.B. Sorokin, G.N. Panin. Nanomaterials, **12**, 4408 (2022). DOI: 10.3390/nano12244408
[35] S. Ullah, X. Yang, H.Q. Ta, M. Hasan, A. Bachmatiuk, K. Tokarska, B. Trzebicka, L. Fu, M.H. Rummeli. Nano Res., **14**, 3756 (2021).
[36] E.V. Emelin, H.D. Cho, V.I. Korepanov, L.A. Varlamova, D.O. Klimchuk, S.V. Erohin, K.V. Larionov, D.Y. Kim, P.B. Sorokin, G.N. Panin. Nanomaterials, **13**, 2978 (2023). DOI: 10.3390/nano13222978

Translated by E.Ilinskaya